Journal of the Korean Nuclear Society
Volume 32, Number 1, pp.77~87, February 2000

Effect of Intercritical Annealing on the Dynamic Strain Aging (DSA) and Toughness of SA106 Gr.C Piping Steel

Joo Suk Lee and In Sup Kim
Korea Advanced Institute of Science and Technology
373-1, Kusong-Dong, Yusong-gu, Taejon, 305-701, Korea

Chi Yong Park and Jin Weon Kim
Korea Electric Power Research Institute
103-16, Munji-Dong, Yusong-gu, Taejon, 305-380, Korea
(Received October 12, 1999)

Abstract

It is reported that the toughness and safety margins of the SA106 Gr.C main steam line piping steel is reduced due to dynamic strain aging (DSA) at the reactor operating temperature for Leak-Before-Break (LBB) application. In this study, intercritical annealing in two-phase ($\alpha+\gamma$) region was performed to investigate the possibility of improving the toughness and reducing DSA susceptibility. The manifestations of DSA were still observed in the tensile tests of the annealed specimens. However, the ductility loss caused by DSA was smaller than that in the as-received material. Furthermore, the intercritical annealing was able to increase the Charpy impact toughness by 1.5 times compared to as-received. With the heat treatment, we could obtain microstructural changes such as the cleaner retained ferrite, increased ferrite content and somewhat finer grain size. It is considered that the reduced DSA was induced by cleaner retained ferrite, which in turn resulted in higher impact toughness in addition to the general toughening due to finer grain sizes and increased ferrite content.

Key Words : intercritical annealing, dynamic strain aging (DSA), SA106 Gr.C, Leak-Before-Break (LBB), impact toughness, retained (old) ferrite, transformed (new) ferrite

1. Introduction

The previous pipe rupture design requirements for nuclear power plant applications are responsible for all the numerous and massive pipe whip restraints and jet shields installed for each plant. These results in significant plant congestion, increased labor costs and radiation dosage for normal maintenance and inspection. In the last decade, however, several experimental and analytical evaluations have shown that the possibility of the hypothetical Double Ended Guillotine Break (DEGB) is extremely low [1]. According to these results, the Leak-Before-Break (LBB) methodology has been applied to design for high energy piping systems by eliminating the

postulation of DEGB. From the point of view on material properties in LBB analysis, the premise of LBB is that the materials used are sufficiently tough that small through-wall crack would remain stable.

The SA106 Gr.C piping steel, however, which was selected for Korea Next Generation Reactor (KNGR) and already used in PWR main steam line piping, and other similar grade carbon steels showed a substantial reduction in toughness due to dynamic strain aging (DSA) at the reactor operating temperature [2, 3]. Therefore, safety margins for the application of LBB concept can be reduced.

DSA is manifested in low carbon steel by serrated stress-strain curves, high work hardening rate, increased strength, negative strain rate sensitivity and reduced ductility at a specific regime of temperature, strain and strain rate [4, 5].

In a certain applications, the strengthening effect of strain aging can be used to advantage such as improved strength, creep and fatigue resistance within DSA temperature range [6]. However, it also exhibited several detrimental features such as decreased ductility and toughness, and increase in the ductile-to-brittle transition temperature (DBTT) .

It is well recognized that effects associated with DSA are caused by interstitial atoms in low carbon steel diffusing during plastic deformation into gliding dislocations or by stress induced ordering of solute atoms thereby lowering misfit energy. Cottrell atmospheres (diffusion induced) or Snock atmospheres (stress induced) develop so called "pinning" or "drag" during dislocation glide which tends to immobilize the dislocations, thus making plastic deformation more difficult. Therefore, dynamic interaction of interstitial atoms and dislocations occurs, thus DSA phenomena appear when temperature is sufficient for diffusion of interstitial atoms to moving dislocations with straining.

Because the amount of dissolved nitrogen or carbon for DSA is extremely small, complete elimination of DSA in carbon steel is difficult, yet, it is possible to control degree of DSA by adding alloying elements or by heat treatment [7].

Since DSA entails interaction between mobile interstitial solutes and dislocations, the solute concentration in ferrite matrix influence the degree of serrated flow characteristic [8]. Therefore, to reduce DSA sensitivity it was suggested that the interstitial solutes content should be reduced. In ferrite matrix of SA106 Gr.C main steam line piping steel, however, which was conventionally produced by normal air cooling after hot extrusion, has relatively high carbon content because of rather fast cooling from the austenite at the hot working temperature. An additional heat treatment, namely, intercitical annealing, was introduced to obtain cleaner ferrite matrix with lower carbon and finer grain size. The dissolved carbon content in the retained ferrite (old-ferrite), which was formed at the $(\alpha+\gamma)$ region, has been known to be lower than that in the transformed ferrite (new-ferrite), which was formed at the pearlite transformation temperature [9].

The purposes of this study are to improve toughness and to reduce DSA susceptibility through intercritical annealing and to give sufficient margins for the LBB applicability of SA106 Gr.C piping steel.

2. Experimental Procedures

2.1. Material Preparation

The SA106 Gr.C carbon steel used in this study was received from Hanjung Co. Ltd, which was the archive material of main steam line piping of

Table 1. Chemical Composition of SA106 Gr.C (w/o)

C	Mn	P	S	Si	Ni	Cr	Mo	V	Al	Cu	Hppm
0.19	1.22	0.009	0.007	0.27	0.11	0.05	0.03	0.004	0.029	0.13	1.6

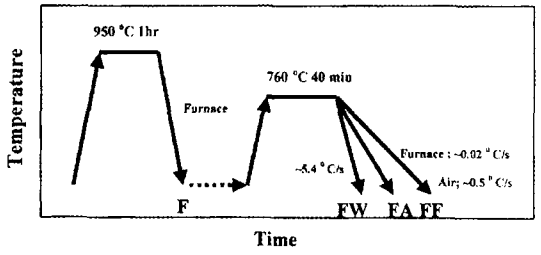

Fig. 1. Schematic Illustration of Applied Thermal History on the SA106 Gr.C Piping Steel

Young Gwang Units 3 and 4 which have dimensions of 669mm outer diameter and 28.6 mm thickness. It was fabricated by normal air cooling after hot drawing. The chemical composition is given in Table 1 and the microstructure was a typical ferrite-pearlite band structure with grain size of 20 micrometer.

2.2. Heat Treatments

As-received SA106 Gr.C, which was normalized after hot drawing of the seamless piping, was homogenized in the austenite range at 950°C for 1hr in a vacuum furnace and furnace cooled. The furnace cooled specimens were designated as F specimen. Then the F specimens were annealed in the intercritical two-phase, namely, ferrite plus austenite phase, field at 760°C. After the annealing for 40 min, the specimens were subjected to air (FA), furnace (FF) and boiling water cooling (FW). The cooling rates from 760°C for the FF, FA and FW specimens were approximately 0.02, 0.5 and 5.4°C/s, respectively. Above stated heat treatment process is illustrated in Fig. 1.

2.3. Fabrication of Specimen and Mechanical Testing

The tensile specimens were machined to an 8mm diameter and 40mm gage length such that their tensile axis was parallel to pipe axis (L-direction). Standard Charpy V-notch impact specimens were machined in the L-C direction by the ASTM E-23 and tested at room temperature. Tensile tests were carried out at various temperatures, from RT to 350°C, and at a strain rates of 1.39×10^{-3}. Specimen temperature was measured by thermocouples, which were welded at upper and lower parts in the specimen, and strain was measured by 0.1 in (0.254cm) extensometer. Tests were performed at universal testing machine (AG-10TA of Shimadzu). Load and displacement were acquired by IBM-PC through A/D converter.

2.4. Metallography and Fractography

The microstructures of SA106-Gr.C, which had the thermal history in Fig. 1, were examined. For metallographic observation, samples were sectioned from the tested tensile specimen shoulder and were prepared using conventional metallographic technique. Nital (2% nitric acid + 98% ethanol) etching and stained boiling alkaline chromate solution (8g CrO_3 + 40g NaOH + 72ml pure water) [10] revealed the microstructures composed of a pearlite and both kinds of ferrite, namely, retained and transformed. Fractography of tensile specimen was taken using a Philips SEM

Table. 2. Average Grain Diameter of the Austenized and Intercritical Annealed Samples

Specimen	Average grain diameter (μm)
F	10.3
FA	8.5
FF	8.8
FW	7.9

515 to examine fracture characteristics. Also, grain size was determined by ASTM E 112-96, general intercept method. These results were shown in Table 2.

3. Results and Discussion

3.1. Microstructures

With the goal of obtaining soft retained ferrite and of improving impact toughness, it is necessary to select a proper intercritical annealing temperature and holding time. According to Andrews' s [11] correlation, it was found that the SA106 Gr.C steel has the lower critical temperature of 716℃. During the intercritical annealing the material was annealed for a long time to develop the paraequilibrium phase, where equilibrium between ferrite and austenite phases are established with respect to carbon, and not with respect to substitutional elements such as manganese [12].

Fig. 2 shows paraequilibrium phase between ferrite and austenite at 760℃. The austenite

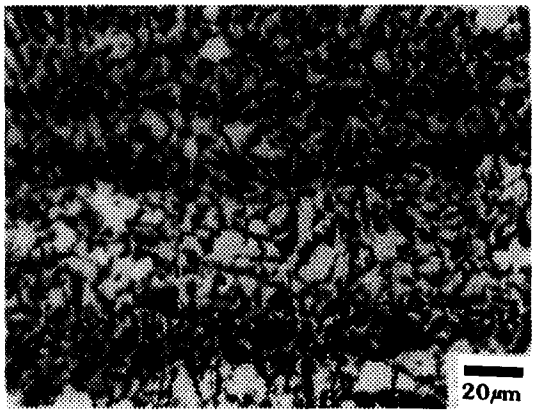

Fig. 2. The Microstructure After Water Quenching from the 760 ℃ After 40min Annealing. The White Areas are Ferrite and the Black Areas are Austenite (martensite). 2% Nital Etched

phase grows along cementite lamella in pearlite bands and ferrite grain boundaries because austenite growth needed high carbon content and easy diffusion path along the grain boundary. The volume fraction of austenite phase was about 65 percent.

Fig. 3 illustrates the optical microstructures developed by the heat treatments F, FA, FF and FW. Fig. 3 (a) shows typical "banding" (alternate layers of ferrite and pearlite) structure. It was reported that banding is primarily due to microsegregation of manganese, non-metallic inclusion and slow cooling rates [13, 14]. Fig. 3 (b) and (c) show the air (FA) and furnace cooled (FF) microstructures after the intercritical annealing. The FA specimen has a narrower pearlite band spacing than the F and FF specimens. It is considered that the FA condition did not give enough time to transform from austenite to ferrite through carbon atom migration, which resulted in narrower pearlite band and grain boundary carbide precipitation. On the other hands, FF condition allowed enough time for carbon atoms to diffuse

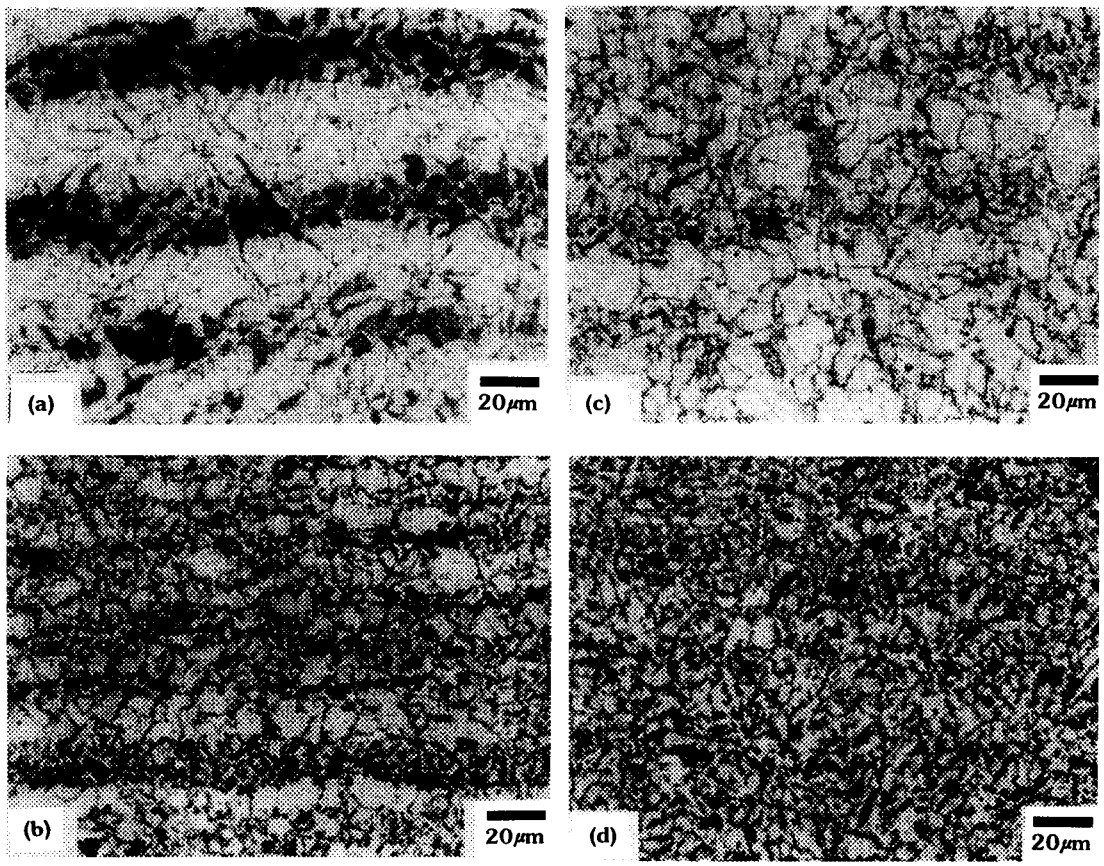

Fig. 3. The Microstructures on Each Heat-treated Condition in SA 106 Gr. C.
(a) F, (b) FA, (c) FF and (d) FW. The White Areas are Ferrite and the Black Areas are Pearlite. 2% Nital Etched

in the austenite during furnace cooling and resulted in a dispersed and some amount of discontinuity of pearlite band layers as ferrite grains are randomly distributed. Also, ferrite content increased due to slow cooling. The FW condition in Fig. 3 (d) has nearly dispersed band structure and acicular ferrite growth due to fast cooling rate.

As listed in Table 2, depending on cooling rate from the intercritical temperature, there are some refinement of grain size and increased pearlite volume fraction.

To distinguish between retained and transformed ferrite, boiling alkaline chromate solution stain [10] was conducted on the specimen FA and FF. The optical micrographs are shown in Fig. 4. The pearlite stained black and the ferrite, which was co-existed with the austenite prior to cooling, stained gray. This ferrite was called retained ferrite. The ferrite formed at cooling from the intercritical annealing temperature, called transformed ferrite, stained white. From the observation of Fig. 4 (a) and (b), transformed ferrite grows epitaxially, there is no grain boundary between transformed and retained ferrite. The remaining austenite was transformed

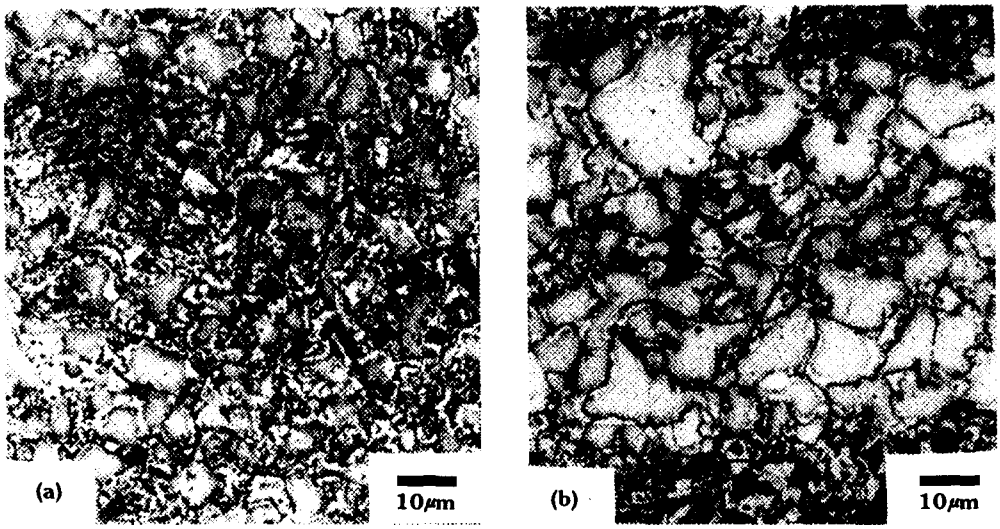

Fig. 4. Optical Micrograph for Steel. (a) FF and (b) FA. The Gray Areas are Retained Ferrite, the White Areas are Transformed Ferrite and the Black Areas are Pearlite. Boiling Alkaline Chromate Solution Stained

to pearlite or carbide precipitation [15].

3.2. Tensile Tests

The results of tensile tests in this investigation displayed typical dynamic strain aging (DSA) phenomena such as occurrence of serrated flow, high work hardening rates, negative strain rate sensitivity, loss of ductility and strengthening.

3.2.1. Stress-strain Curves

In the stress strain curves, the serrated flow behavior has been observed at a certain combination of temperature and strain rate, but the stress amplitude in serrated flow was relatively small compared to other similar grade carbon steels [2]. This reduced sensitivity on DSA phenomena was also observed at the as-received SA106 Gr.C [3] and seems to be related to high manganese content [16].

Fig. 5 shows the effects of temperature on stress-strain curves at a strain rate of $1.39 \times 10^{-3}s^{-1}$. From the figure observation, typical Luder's strain occurred at the lower temperature and disappeared with increasing temperature. In the case of FW the Luder' s strain was not observed even at the room temperature. This disappearance of yield point phenomena were thought to be caused by the high dislocation density related to fast cooling rate, about 5.4℃/s, after the intercritical annealing. It was supported by the fact that stress-strain curves exhibited high work hardening and general drop of yield stress at high temperatures was not severe. Dual phase (ferrite plus martensite) steels show the disappearance of yield point phenomena and the high work hardening rate due to the same reason [17].

At the fast cooling rate of FW, maximum serration peaks occurred at the lower temperature, while the maximum peaks for other specimens occurred nearly at the same temperature region,

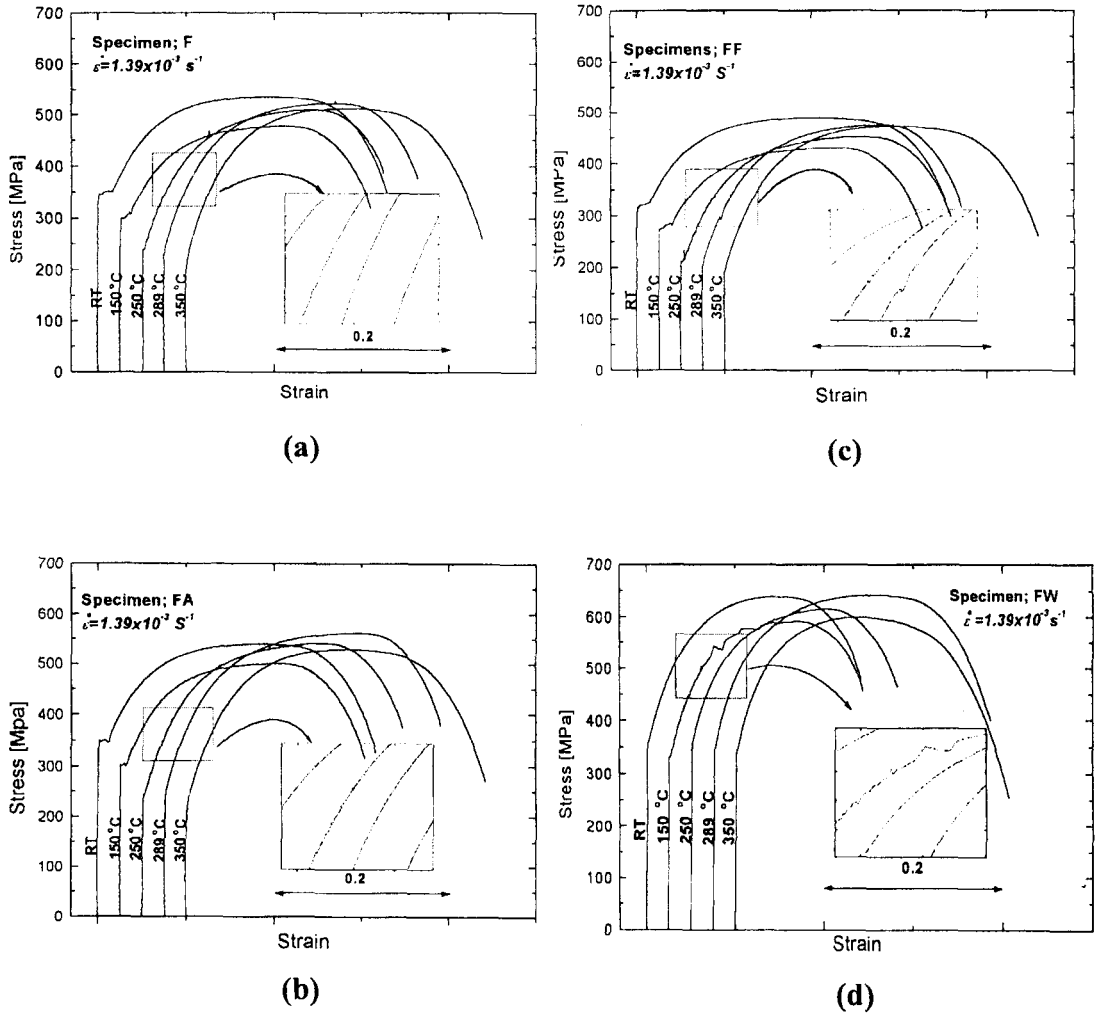

Fig. 5. Stress-strain Curves at Various Temperatures at a Strain Rate of $1.39 \times 10^{-3}s^{-1}$ of Heat-treated Specimens. (a) F, (b) FA, (c) FF and (d) FW

about 250℃. It is understood that the amount of mobile dislocations in the FW condition are higher than that in the other heat-treated conditions due to rapid cooling and fine-grained which produce more dislocation at the same amount of plastic deformation [15, 17]. Therefore, the average velocity of moving dislocations is lower (Cottrell' s model [18, 19]). In other words, the waiting time of the dislocations in front of obstacles is longer than the other heat-treated conditions (McCormick' s model [20, 21]) in addition to the increased interstitial solute content by the rapid cooling rate. Therefore, the possibility of locking during dislocation glide by the interstitial atoms increased, and which resulted in more apparent serration peaks at lower temperature.

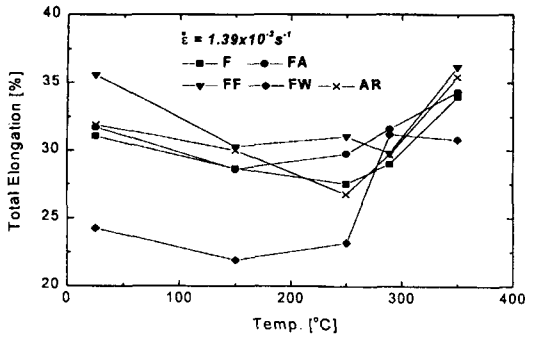

(a)

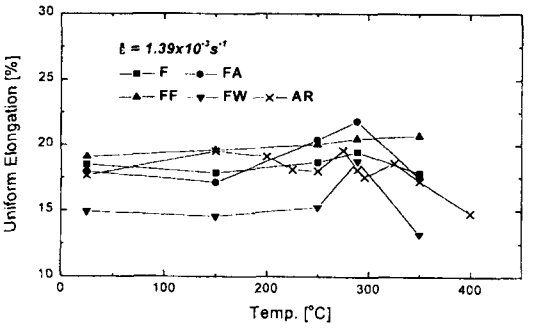

(b)

Fig. 6. Comparison of Elongation of as-received and Heat-treated Specimens at a Strain Rate of $1.39 \times 10^{-3}s^{-1}$. (a) Tatal Elongation and (b) Uniform Elongation

3.2.2. Effect of Intercritical Annealing Treatment

To investigate the effects of intercritical annealing treatment, total and uniform elongation were compared for the same strain rate on each heat-treated specimen. Fig. 6 (a) and (b) shows the change in elongation at various temperatures. In this figure, FF specimen shows a higher ductility than the others in all test conditions. As increasing test temperature, FA condition resulted in higher elongation than F condition, namely, FA had been less affected by DSA than F. From the result of reduction of area it obviously shows the degree of

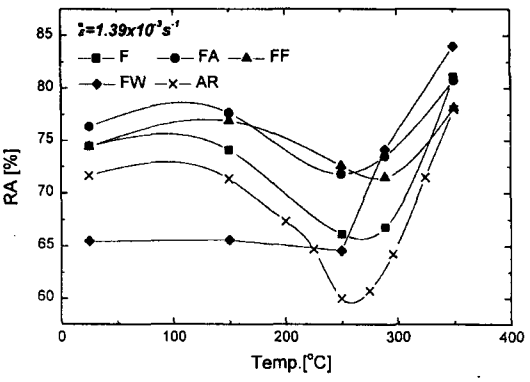

Fig. 7. Comparison of Reduction in Cross-section Area Between as-received [3] and Heat-treated Specimens at a Strain Rate of $1.39 \times 10^{-3}s^{-1}$

ductility loss. According to the Fig. 7, loss of reduction of area due to DSA was the most significant at the as-received material. Since F was slowly furnace cooled from 950℃, the F condition exhibited relatively small amount of ductility loss compared to as-received material. Even F had less affected by DSA than as-received, the F condition shows more ductility loss than intercritically annealed FF and FA conditions. It could be explained by the fact that soft retained ferrite and dispersed pearlite band formed by the intercritical annealing gave higher ductility than the F condition. From the Fe-C phase diagram, it is evident that the carbon content in the retained ferrite, which was formed at the $(\alpha+\gamma)$ region, may be lower than that the transformed ferrite, which was formed at lower temperature [9].

3.3. Fractography and Charpy Impact Test

All of tensile-tested specimens in this study were the typical ductile "cup and cone" fracture. Fig. 8 shows a photograph of the fracture surface of FF specimen with temperature at RT, 250 and 350℃ for strain rate of 1.39×10^{-3} s^{-1}. There was no

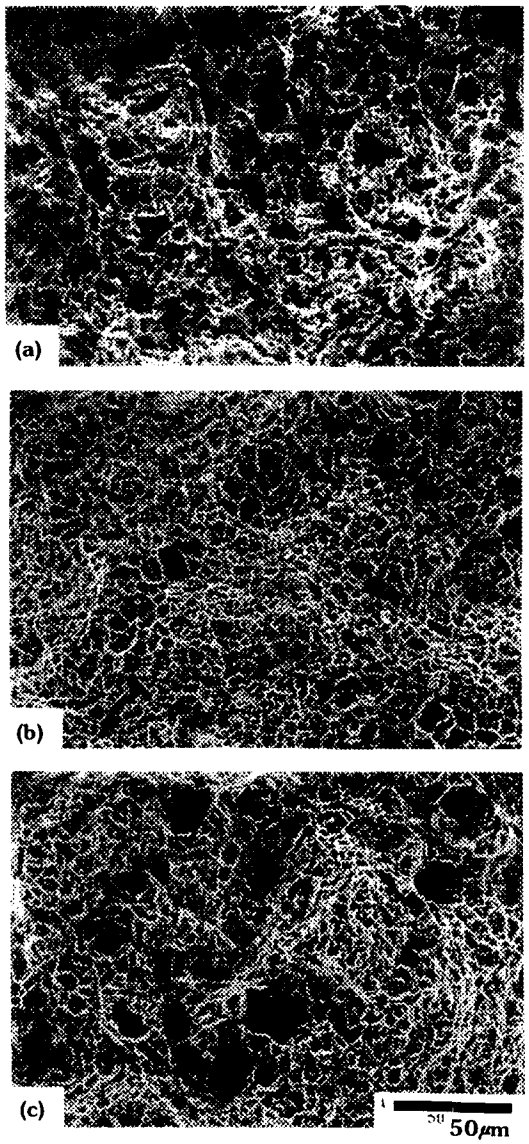

Fig. 8. SEM Photographs of Fracture Surface in FF Specimens. (a) RT, (b) 250 and (c) 350℃

significant variation of appearance with temperature, all the fracture surfaces exhibit "dimpling", a feature often observed on ductile fracture surfaces. However, the low ductility fracture surfaces here in 250℃ contained shallow

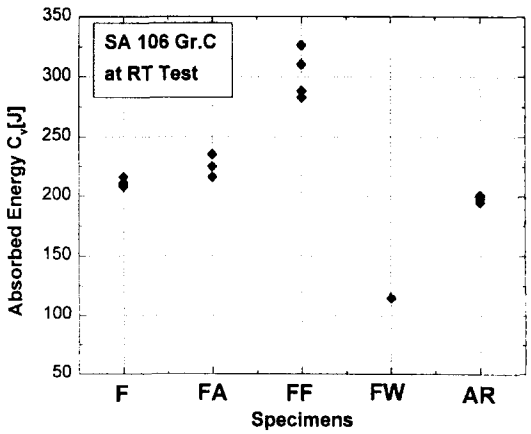

Fig. 9. Charpy Impact Test at Room Temperature of Heat-Treated Specimens

and small size of dimple compared at RT and 350℃

Generally, ductile fracture in metals and alloys is frequently initiated by the fracturing of precipitates [22] or inclusions or by their parting from the matrix [23], final failure then arises as a consequence of the coalescence of voids formed in this way. As the amount of deformation increases, the voids become elongated in the tensile direction. At the same time fine voids formed at the small carbide particles or inclusions and these join up. In case of DSA affected, however, it was supposed that these fine voids could not fully join up and become larger since increased strain hardening caused by DSA would not allow fully plastic deformation to join up with neighboring voids.

Standard Charpy V-notch (CVN) impact tests were performed at room temperature. As can be seen in Fig. 9, the furnace cooled specimens after intercritical annealing (FF) showed higher toughness by 1.5 times as compared to other heat-treated conditions. It could be explained that increased ferrite content and clean (lower interstitial carbon content) retained ferrite [9]

which were produced by slow cooling after intercritical annealing might have caused the higher impact toughness and ductility in addition to the general toughening due to somewhat finer grain sizes. These trends show agreement with tensile test results at room temperature.

4. Conclusions

The effects of intercritical annealing on the mechanical properties of SA106 Gr.C piping steel were investigated through the tensile and Charpy impact test. The main conclusions are as follows.

1. After intercritical annealing treatment, we were able to obtain both kinds of ferrite, namely, retained and transformed. Furnace cooled specimens after intercritical annealing shows more amount of ferrite content and dispersed pearlite band than that in the air-cooled or boiling water-cooled specimens.
2. In all heat treatments, DSA phenomena in SA106 Gr.C were observed in tensile properties. However, the magnitude of serration and the strength increased by DSA were relatively small compared to similar grade carbon steels. In case of increasing cooling rate from intercritical temperature, the maximum serration peaks shifted to lower temperature.
3. Intercritical annealing treatment gives less DSA. In furnace-cooled specimens after intercritical annealing, total elongation showed higher than that in the others. At the reactor operating temperature, intercritical annealing treatment resulted in somewhat higher elongation than the as-received or furnace-cooled specimens after austenizing.
4. The furnace cooled condition after intercritical annealing showed about 50% increase in the impact toughness compared to the others.

Acknowledgment

The authors are grateful to the Korea Insititute of Nuclear Safety (KINS) for the financial support.

References

1. D. O. Harris, E. Y. Lim, and D. D. Dedhia, *NUREC/CR-2189*, **5**, Nuclear Regulatory Commission (1981).
2. C. W. Marschall, R. Mohan, P. Krishnaswamy and G. M. Wilkowski, *NUREG/CR-6226*, October (1994).
3. J. W. Kim, and I. S. Kim, *Nuclear Engineering and Design*, **172**, PP. 49~59 (1997).
4. A. R. Rosenfield et al, *Dislocation Dynamics*, pp. 381, McGrow-Hill, New York (1968).
5. R. E. Reed-Hill. *The Inhomogenity of Plastic Deformation*, pp. 191, ASM, Metal Park., Ohio (1973).
6. J. D. Baird, *Metallugical Reviews*, **16**, 1, (1971).
7. W. C. Lesile and R. L. Rickett, *Trans. of AIME*, Aug., pp. 1021 (1953).
8. B. Russel, *Philos. Mag.*, **8**, pp. 615 (1963).
9. J. J. Yi and I. S. Kim, *Scripta METALLURGICA*, **17**, pp. 299~302 (1983).
10. R. D. Lawson, et al., *Metallography*, **13**, pp. 71 (1980).
11. K. W. Andrews, *JISI*, **203** (7), July, pp. 721~727 (1965).
12. J. B. Gilmour et al., *Met. Trans.*, **3**, pp. 1455~1464 (1972).
13. S. W. Thomson, P. R. Howel, *Mater. Sci. Technol.*, **8**, pp. 777~784 (1992).
14. C. Thaulow, et al., *Eng. Fracture Mech.*, **24**, pp. 263~276 (1986).
15. Matlock, D. K., et al., *Structure and Properties of Dual-Phase Steels*, pp. 62~90, AIME, New York (1979).

16. C. C. Li and W. C. Leslie, *Metall. Trans. A.* **9A**, pp. 1765 (1978).
17. R. A. Kot, et al. *Fundmentals of Duel-Phase Steels*, AIME (1981).
18. A. H. Cottrell, *Dislocation and Plastic Flow in Crystals*, Clarendon Press, Oxford (1953).
19. A. H. Cottrell, *Philos. Mag.*, **74**, pp. 829, (1953).
20. P. G. McCormick, *Acta Mettall.*, **20**, pp. 351 (1972).
21. P. G. McCormick, *Scripta Mettall.*, **7**, pp. 945 (1973).
22. J. T. Barnby, *Acta Metall.*, **15**, pp. 903 (1967).
23. K. E. Puttick, *Phil. Mag.*, **4**, pp. 964 (1959).